Supplementary Information for

Large Field of View Fluorescence Imaging of Microfluidic Devices with a Tandem-Lens Macroscope

Daniel A. Mokhtari[a,b,*], Ali Lashkaripour,[a], and Polly M. Fordyce[c,d,e,f*]

[a] *Velocity Bio, Inc., 733 Industrial Rd, San Carlos, CA, USA.*
[b] *Previous Affiliation: Department of Genetics, Stanford University, Stanford, CA, USA.*
[c] *Department of Genetics, Stanford University, Stanford, CA, USA.*
[d] *Department of Bioengineering, Stanford University, Stanford, CA, USA.*
[e] *Sarafan ChEM-H, Stanford University, Stanford, CA, USA.*
[f] *Chan-Zuckerberg Biohub, San Francisco, CA, USA.*
[*] *Corresponding authors: daniel.mokhtari@velocitybio.tech & pfordyce@stanford.edu*

Contents

Materials and Methods

Macroscope imaging system construction

Design rationale and build summary

A macroscope build list of components and their prices (as of early 2024, with the exception of new stage components which are as of early 2026) is provided in Table S1. For second-hand components, approximate prices based on listings as of early 2024 are given. The build description below generally references parts by name, and specific part numbers, manufacturers, and vendors can be found in the build list.

Motion control. The macroscope utilizes a motorized stage system providing high-precision (sub-micron) XYZ motion control with high-quality linear encoders with build inspired from an ASI manufacturer manual for the ASI LS-Series linear positioning stages (*1*). This type of motion control system can be purchased for approximately $15,000 USD new, but high-precision second-hand stages can be sourced at significantly lower cost. Thus, we built a complete XYZ motion control system from high-accuracy second-hand ASI components, including a motion controller with serial computer interface (ASI LX-4000). This build can routinely be achieved from the second hand market at a total cost of approximately $2,500 USD. This motion control system enables long range of travel ($100\times100\times50$ mm) and highly-precise (sub-micron repeatability) XYZ control for up to three 1×3 inch slides, and thus three HT-MEK microfluidic chips, simultaneously.

Excitation light treatment. The macroscope's optical train utilizes a standard liquid light guide to route output from an incoherent, high-powered, LED light source. In our build, we used a state-of-the-art Lumencor SPECTRA III light engine since this light source was on hand and offered bright, multi-channel illumination perfect for optical system development. This specific light engine is not necessary to complete this build, and multi-wavelength light sources with similar core features in fewer channels (e.g., Thorlabs CHROLIS 6-channel source or Thorlabs LED4D 4-Wavelength source) can be purchased at substantially lower cost (approximately $12,500 USD and $6,700 USD, respectively, as of Fall 2025). A liquid light guide enabled interfacing with a wide variety of light sources without altering mounts and provided flexibility in system packaging (placing the source outside of an enclosure, for example). Transmitted light is collimated at the top of the macroscope optical train, then expanded with a commercial fly's eye homogenizer to create a rectangular output with approximately top-hat intensity profile spanning the large image circle of the lens system. This approach was found to be superior to a simple Galilean beam expander, providing a significantly more uniform beam profile and higher irradiance at the sample plane.

The shaped excitation beam is then filtered through a 50-mm-diameter OD6 bandpass excitation filter (fluorescence bandpass filters used were from Chroma Technology Corp.) mounted in a low-profile electronic filter wheel (ZWO Astro) with 5 filter slots, equipped with DAPI, GFP, and Cy5-compatible excitation filters in our default configuration. Filtered excitation light is aligned with the central axis of the lens system below and positioned to approximately focus the homogenizer output at the imaging front focal plane. To

achieve bright-field imaging on the macroscope, we used multi-channel excitation in red, greed, and blue channels simultaneously at very low power. We attenuated the excitation light beam with an OD 2.0 absorptive ND filter (Thorlabs) loaded in the excitation filter wheel, and used an empty emission filter cell to pass all transmitted light to the camera sensor.

Emission light treatment. Emitted light from the imaging front focal plane is collected via a finite-corrected optical system utilizing a face-to-face, tandem-lens macro configuration related to previously described systems (*2*). Our system differs from most other reported tandem-lens macro configurations in that we use a symmetric configuration with the same lens on both sides. This symmetric configuration produces an approximately 1:1 image (1X magnification) of the sample on the camera sensor, and was selected to produce a very large image circle. In this type of system, each lens is set at infinity focus, them mechanically coupled face to face such that the "sensor side" of each lens is sitting outward. This configuration can produce extremely shallow (down to low micron) depth of field and produce a sharp image across a very large (10s of mm) field of view.

To build our lens system, we considered several fast, full-frame sensor compatible, and F-mount compatible commercial lenses with manual aperture and focus control (Zeiss Milvus ZF.2 50mm f/1.4, Rokinon 85mm f/1.4 ASPH, Rokinon 85mm f/1.4 Series II, and Nikon Nikkor 50mm f/1.2 lenses) and qualitatively assessed their performance on an early prototype of our macroscope system by evaluating image circle diameter, vignetting, and aberration. The degree of hard vignetting, and thus the final image circle seen on the sensor, soft vignetting, and spherical aberration, were found to vary widely lens to lens due to differences in internal lens architecture and face diameter. We settled on the Rokinon 85mm f/1.4 Series II lens because it yielded a good tradeoff of cost, compactness, apparent numerical aperture, and front face diameter (which was an important constraint for emission filter wheel mounting). We noted in our testing that extremely fast lenses (i.e., f/1.2) produced depths of fields so shallow that field curvature (Petzval curvature) became very noticeable, and it also became challenging to reliably align the stage sample plane with the focal plane. Incorporating additional axes of precise stage motion adjustment could make these faster, and thus higher numerical aperture, lens systems more appealing for use in our macroscope system from the perspective of aligning sample and lens focal planes, but custom optics would be required to reduce the field curvature.

Emission filtering was performed within the approximately infinity-corrected space between the tandem lenses to minimize distortion. Since hard vignetting was seen to worsen (image circle reduces) as a function of tandem lens separation, we minimized separation of the lenses by directly mounting a second 5-position low-profile electronic filter wheel to the front faces of (between) the tandem lenses. Since excitation light shines directly into the lens system, we stacked two (2) identical OD6 bandpass emission filters face-to-face within the filter wheel using a custom filter cell and spacer (Fig. S1).

Choice of a transillumination optical system

By utilizing a trans-illumination configuration, our system can maintain a larger field of view than would have been possible by using epi-illumination. This is because with a

dichroic positioned between the tandem lenses, lenses would have to be separated by a much larger distance, which would increase the degree of hard vignetting (clipping) and thus reduce the diameter of the image circle produced on the sensor. In addition, although including a second emission filter per channel to adequately block excitation light in our trans-illumination system incurs additional costs, our approach offsets that cost by dispensing with a dichroic mirror and mounts (cubes) required to co-align paired filters and a dichroic.

Choice of imaging camera

We selected a camera designed for astrophotography (ZWO, ASI6200MM Pro) to cost-effectively meet the needs of our imaging application. This camera, and other similar astrophotography cameras, offer very large (i.e., full-frame, 8K-resolution) CMOS based sensors with 16-bit analog-to-digital converters and active cooling with high peak quantum efficiency (>90%), while offering favorable maximum frame rates (2 Hz) at modest cost (~$4,000 USD). In comparison, high-performance scientific cameras (e.g., Teledyne Photometrics Kinetix, Teledyne Vision Solutions) for several times the price offer some similar features but offer very high speed readout and data transfer rates (>80 FPS full-frame readout in high-dynamic range mode) that are often not required for microfluidic applications. In addition, most possess significantly smaller and lower resolution sensors (the majority of sCMOS sensors on the market are <3200×3200 pixels).

Software control

The light source, excitation filter wheel, XYZ stage, emission filter wheel, and camera are controlled and synchronized using the Micro-Manager open source microscope control software package (*3*). By using Micro-Manager and configuration presets, this macroscope imaging system was easily interfaced with an existing, previously-described Python package capable of scripted and coordinated microfludic valve control and imaging (*4*). By abstracting hardware-level configuration and communication behind Micro-Manager presets and API calls, our macroscope can be easily upgraded and extended with additional commercial components without requiring significant changes to custom automation code. Additionally, since high-intensity unfiltered excitation light focused on the sensor could damage the camera, use of Micro-Manager presets that match the excitation and emission filters with corresponding light source channel and appropriate output power prevents accidental system damage.

Epifluorescence microscope comparison systems

Nikon Ti2 based widefield setup used in this study

As a comparison imaging system for benchmarking, we used a commercial, state-of-the-art, motorized Nikon ECLIPSE Ti2-E inverted epifluorescence microscope system equipped with extremely high-end components. This microscope was equipped with a high-resolution motorized ASI XY stage, motorized focus control (Z-stage), a Lumencor SOLA U-N solid-state white light source, a Teledyne Vision Solutions Photometrics

Kinetix camera, and Nikon high signal-to-noise BL Series (large FOV) fluorescence filter cubes. These Nikon filter cubes contained Semrock (IDEX Health & Science) bandpass filters and dichroic mirrors (spectral properties and part numbers provided in Table S3). We used 2X and 4X objectives of the highest numerical aperture readily available (Nikon CFI Plan Apo Lambda D series) and we used the only available Nikon 1X objective (CFI Plan Achro, Table S2). At the time of purchase, this system had a total price of over $100,000 USD. If equipped with a Lumencor SPECTRA III light source, as used for the macroscope build, the total price of this system would have been approximately $115,000 USD.

Other commercial imaging systems

Besides inverted microscopes like the Nikon Ti2, other turnkey commercial systems could offer large-FOV epifluorescence imaging at a similar or lower price point. Two such systems are the Nikon SMZ25 and Evident MVX10 stereo microscopes, which offer advantages over traditional inverted epifluorescence imaging systems for wide FOV imaging. These systems use low-magnification objectives with significantly better light-gathering ability than standard microscope objectives (e.g., Nikon P2-SHR Plan Apo 0.5X/0.78 and Evident MVPLAPO 1 X 1X/0.2 objectives), combined with long working distances ($\geq$60 mm with 1X Objectives). These systems are also designed for epifluorescence imaging and can accommodate automated filter turrets and motorized z-position (and focus) control, making them possible alternatives to the macroscope for high-sensitivity large FOV imaging. However, these turnkey systems have limitations that significantly compromise their use for the applications around which the macroscope was designed.

Generally, these systems are optimized for zoom stereoscopic applications instead of fixed-magnification monoscopic ones like those the macroscope is designed to serve. This incurs unnecessary cost and compromises performance for the microfluidic use cases described herein. Additionally, these systems can't be specified "out of the box" to offer all of the features of the macroscope system described here. For example, the Nikon SMZ25 has no first-party catalog motorized XY-stage on offer.

In terms of light gathering performance, literature suggests these commercial systems suffer from poorer fluorescence imaging performance (i.e., NA) than their paper specifications might indicate. As noted in prior literature evaluating the the Olympus (Evident) MVX10 system for a custom wide FOV imaging application using the MVPLAPO 2 XC (2X) high NA objective, light-gathering at low magnification within the zoom body was significantly degraded, suggesting that apparent NA at low magnification is lower than suggested by the nominal NA of the objective alone (*5*). This observation led the authors to develop an alternative imaging path instead of using the MVX10 body. We estimate that our lens system provides a numerical aperture of 0.2–0.3, which is on par with or superior to Nikon or Olympus stereo microscope objectives at the same magnification (Nikon P2-SHR Plan Apo 1X: NA = 0.156, MVPLAPO 1 X: NA = 0.25). In terms of field of view at 1X magnification, our system is superior to Nikon SMZ25 because the Nikon system's system filter wheel accommodates 25 mm filter sets; assuming no image enlargement after emission filtering, the maximum achievable FOV at 1X magnification of this system is approximately 25 mm in diameter. This is significantly less (25% smaller image circle diameter and 34% smaller imaging region area) than the 34 mm diameter and 740 mm^2

FOV our system can achieve at the same magnification.

These stereo microscope systems cost less than the fully-equipped Ti2 test system but are still significantly more expensive than the cost of the macroscope. For a new SMZ25 system, online reseller pricing is approximately $53,000 when equipped for GFP and RFP-channel fluorescence imaging; it is unclear if that quoted system had a manual or motorized filter wheel, and that system did not appear to include a camera or light source and does not include a motorized XY stage solution (which isn't available from Nikon). Comparing this system vs our "all new" macroscope build cost, and adding on the price of the new XY stage system and controller we specified in our build, the new Nikon system from this vendor would cost approximately twice as much as our "all new" system build. With the addition of a fit-for-purpose multi-channel and high-powered light source and driver (e.g., Thorlabs 4-Wavelength High-Power LED Source, LED4DXXX, and suitable driver, DC4100, at approximately $7,000 total), we estimate price the of a macroscope-comparable Nikon SMZ25 system would be approx. $72,000, 90% above the macroscope build detailed herein with the same light source ($38,000 "all new").

Finally, the macroscope system can be customized for particular applications more readily and at lower cost than the Nikon or Olympus systems. As examples, 1) a larger motorized filter wheel can be fit to our custom system to handle more fluorescence channels (e.g., ZWO EFW-7x2-25, which can accommodate 7 filter cells), and 2) our system can be built with various motorized z-axis stages to meet the precision demands of particular applications. These modifications are not possible on the Nikon or Olympus system with non-custom first-party components, and would likely require significant customization of the microscope body or fabrication of custom parts to retrofit.

HT-MEK microfluidic device fabrication

The two-layer PDMS devices (HT-MEK chips) used here were fabricated as previously described from casting of photolithographically-produced silicon wafer molds, also made as previously described (*6*). Device and mold fabrication were performed within class 10,000 and class 1,000 clean rooms, respectively.

On-chip fluorescence standard curves

Fluorophore stock preparation

Dilution series of fluorescein disodium salt (VWR cat. no. 97062-186), 6,8-difluoro-7-hydroxy-4-methylcoumarin (DiFMU, ThermoFisher Scientific, cat. no. D6566), and Cyanine5 (Cy5, MedChem Express, cat. no. HY-D0821) dyes were prepared in 1X phosphate-buffered saline (PBS, ThermoFisher Scientific, cat. no. 10010023) from concentrated stocks in anhydrous dimethyl sulfoxide (DMSO, ThermoFisher Scientific, cat. no. D12345). Each standard was prepared as a serial dilution at the following concentrations (μM): 0, 0.02, 0.1, 0.5, 2.5, 12.5, and 62.5. For some imaging exposure times, 62.5 μM of fluorophore saturated the camera sensor, in which case that concentration was omitted from downstream analyses.

Device setup

Brightfield images were acquired with dry (*i.e.*, no fluidic control lines were connected) HT-MEK chips on both the macroscope and our benchmark Ti2-based imaging system. For fluorophore dilution series imaging, pressurized fluidic control lines containing water were connected to the chips as previously described (*7*).

Device imaging

Image acquisition. Imaging and fluidic control of chips for dilution series was scripted using the customized Python-based hardware automation framework described above (Software control) within a Jupyter Notebook. The working distance of the lens system was found to have small dependencies on the fluorescence channel used (emission filter identity) with differences on the order of approximately $\leq$100 µm. To account for this, we measured offsets in imaging system focus Z-positions using a low concentration of each fluorophore and the corresponding filter cube. These offsets were coded into the standard curve acquisition scripts so that images for each standard were taken at the optimal Z-position corresponding to that channel. A 10% overlap between tiles was used for all images acquired on the benchmarking Ti2 setup using 2X or 4X objectives.

Flat-field correction and stitching. Images taken on both the macroscope and Ti2 were first flat-field corrected to remove vignetting-dependent brightness differences across the field of view. Flat-field correction was performed as previously described (*4*). Briefly, flat-field images were acquired on both imaging apparatuses by taking images of concentrated fluorophore used in each standard series in its respective imaging channel. Correction was then applied as previously described (*8*). Flat-field corrected images acquired on the Ti2 equipped with a 2X or 4X objective were then "stitched" to construct a complete chip image using a custom Python package previously reported (*4*). As images acquired on the macroscope and on the Ti2 equipped with the 1X objective contained the entire region of interest, no tiling was required in these cases. Then, images were subjected to feature finding (chamber edge detection) and fluorescence intensity quantification, producing summary reports of apparent fluorescence intensity within each chamber at each concentration point. Image processing was also performed with a custom Python package in a Jupyter Notebook as previously reported (*4*).

Intensity normalization. For standard curves of fluorophore within the HT-MEK chip, median chamber intensities at each fluorophore concentration were divided by the median intensity in the presence of no fluorophore ("background") to yield normalized intensities ("signal response") used for standard curve plotting and linear fitting. Normalization was performed on a per-chamber basis.

Fluorescent bead standard series

A commercial standard series of fluorescent beads at 6 relative intensities (Thermo Fisher InSpeck Green 6 µm beads, cat. no. I14785) was imaged to quantify signal-to-noise (SNR)

of the macroscope and Ti2 comparison system equipped with different objectives.

Sample slide preparation and imaging

Beads at each relative intensity were diluted 1:10 in water, and 5 μL of bead suspension was spread out on a 22mm square cover slip and allowed to dry. Then, 10 μL of mounting medium was placed on a glass slide, the cover slip with dried beads was placed atop under light pressure, and slides were sealed with nail polish. Slides were imaged on the macroscope as well as the Ti2 with 1X, 2X, and 4X objectives, each in the GFP channel with 40 ms exposure.

Image Analysis

Preprocessing. Images of fluorescent beads at decreasing relative intensities (manufactured with different fluorophore concentrations to yield a standard series of fluorescence intensities) were processed to identify beads, extract their intensities, and define and quantify their local backgrounds. To do this, we flat-field corrected the macroscope images as well as the images acquired with the 1X objective on the Ti2, as vignetting for these images was substantial compared to the higher-magnification objectives. For the macroscope images, we cropped to an ROI containing the beads, which was a central subregion 4200x4200 pixels. For the Ti2 images, we cropped slightly to an ROI about 10% smaller than the full sensor image to remove lingering vignetting at the image corners.

Bead finding. Each processed image was manually thresholded to separate beads from background and the "Analyze Particles" function of ImageJ/Fiji was used to define bead ROIs. A local background ROI was defined for each bead as the region enclosed between the bead ROI border scaled up by 2- and 4-fold, respectively. Image intensities (ADUs) within the bead ROIs and local background ROIs were extracted for each bead and used for subsequent calculation of SNR.

SNR calculation. We removed measurements likely arising from beads that were touching or very close to one another. This was achieved by visualizing distributions of the standard deviation of local background ADU values for each bead, from which we defined manual culling thresholds based on standard deviation values (removing beads above that threshold from further analysis). This procedure was applied for each each imaging system and objective. With the remaining data, we calculated per-particle SNR from pixel ADU values as follows: $\mathrm{SNR}_{\mathrm{Particle}} = \frac{\text{Mean(Particle)-Mean(Background)}}{\text{Stdev(Background)}} = \frac{\text{Net Signal}}{\text{Background Spread}}$. We also calculated mean SNR for a given sample across beads as follows: $\mathrm{SNR}_{\mathrm{Mean}} = \frac{\text{Mean(Net Signal)}}{\text{Mean(Background Spread)}}$.

PafA turnover assay

PafA construct design and cloning

A fusion construct of PafA phosphatase (Uniprot ID Q9KJX5) and monomeric eGFP (mEGFP) was designed for *in-vitro* transcription/translation (IVTT) with PURExpress (New England Biolabs). This expression construct was generated from a synthesized gene block (Integrated DNA Technologies) consisting of a methionine start codon followed by codons for residues 21–546 of PafA phosphatase, codon-optimized for *E. coli*, cloned into a backbone vector (PURExpress DHFR Control Plasmid, New England Biolabs, with DHFR coding sequence removed) containing a downstream flexible Ser/Gly linker (amino acid sequence "-GGGSGGGGSG-") and fused C-terminal mEGFP. Cloning was performed via HiFi assembly (New England Biolabs) with linearized vector bearing complementary overhangs, and sequence-verified, miniprepped plasmid was used for downstream IVTT.

Device setup and patterning

An HT-MEK chip was pressurized and surface patterned to immobilize a patch of anti-eGFP antibody on the surface within each chamber, as previously reported (*4*).

PafA expression, purification, and assay with HT-MEK

Off-chip cell-free expression and on-chip purification. PafA-mEGFP fusion was expressed off-chip via *in vitro* transcription-translation (IVTT) with PURExpress reconstituted cell-free expression system (New England Biolabs, cat. no. E6800L), and this expression mixture was then flowed over one-half of a patterned HT-MEK chip to immobilize and purify the expressed enzyme. First, an 18 µL expression reaction was prepared on ice by combining 14 µL of a master mix consisting of 4:3 parts PURExpress components A and B, 1 µL of recombinant RNAse Inhibitor (Promega, cat. no. N2511) at 16 U/µL, 2 µL of plasmid DNA template at ~50 ng/µL, and 1 µL of $ZnCl_2$ at 2 mM in water. This reaction was incubated in a thermocycler for 2 hours at 37 ºC, then 1 hour at 23 ºC to express PafA fusion protein. Then, the IVTT reaction was diluted 5-fold into a buffer consisting of 100 mM MOPS, 500 mM NaCl, 100 µM $ZnCl_2$, and 1 mg/mL BSA at pH 8.0 (1X PafA Reaction Buffer), and this IVTT dilution was flowed over the patterned HT-MEK chip for about 10 min with the button valves in the open state. Following binding, excess unbound enzyme was flushed out of the chip by flowing 1X PafA Reaction Buffer for an additional 10 min with the button valves closed, and bound enzyme was visualized on the macroscope by imaging in the GFP channel.

SDS wash to remove contaminating enzyme. The chip was washed with an SDS solution, similarly to previously reported, to remove contaminating PafA non-specifically bound to chamber walls (*4*). This wash denatures and inactivates PafA that is not mechanically protected by (specifically recruited beneath) a valve within each chamber. To do this, a solution of 1% SDS in 1 M HEPES buffer at pH 7.3 was flushed continuously through the chip for 20 minutes with these enzyme-bearing valves closed. Then, the chip was flushed copiously with 1X PafA Reaction Buffer prior to turnover assays.

On-chip turnover assay with DiFMUP. A kinetic time-series turnover assay was performed on the chip containing surface-recruited and purified PafA using 6,8-difluoro-4-methylumbelliferyl phosphate (DiFMUP, AAT Bioquest, cat. no. 11627) substrate. DiFMUP is an activated fluorogenic phosphomonoester substrate similar to previously reported coumarin substrates of PafA, and was expected to be rapidly hydrolyzed by PafA (*4*). A concentrated stock solution of DiFMUP in DMSO was used to generate a 50 μM stock of DiFMUP in 1X PafA Reaction Buffer. This DiFMUP solution was flowed through the chip for about 8 minutes with enzyme-bearing valves closed (to avoid cleaving substrate prematurely), and then these valves were opened to expose enzyme and initiate reactions while valves separating adjacent chambers were simultaneously shut. Rapid imaging was then initiated (as described above, Software control) in the DAPI channel with 50 ms exposure times to quantify fluorescent product (DiFMU) generation over time.

Turnover image analysis

Image processing of macroscope DAPI-channel images from DiFMUP turnover kinetic timecourses was performed as previously reported to extract median chamber intensities for all images at each timepoint (*4*). These intensities were background intensity (intensity at t = 0 s after reaction initiation) subtracted and normalized to the final intensity (at complete product turnover) to generate relative turnover curves used to assess accuracy of initial rate fitting across each chamber. Linear least-squares fitting was performed to estimate initial rates.

Simulated temporal downsampling

We temporally down-sampled the macroscope-acquired PafA turnover data (Fig. 4C) to approximate, or simulate, the imaging data that would be acquired using a 2X objective on the Ti2 microscope. To do this, we used empirically determined tiled imaging times using a reference HT-MEK chip collected using the 2X objective on the Ti2. The sampling rate of the simulation varies slightly over the imaging session because 1) the time to reach the same spatial position in the tiled series is not perfectly constant on the Ti2 due to software-controlled hardware blocking (delays arise from stage movement, image transfer over the USB bus, and other reasons), 2) the imaging rate on the macroscope is not constant for the same reasons (in Fig. 4C, the image thumbnails are indexed but those indices do not correspond to identical time deltas between images), and 3) we rounded to the nearest imaging timepoint from the macroscope data for each simulated Ti2 observation.

Figures S1 to S10

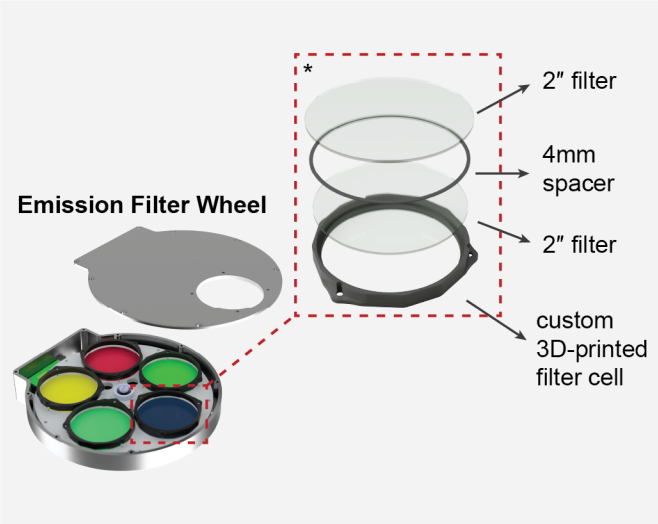

Fig. S1. Motorized emission filter wheel assembly containing two stacked OD6 bandpass filters housed in a custom filter cell for each channel.

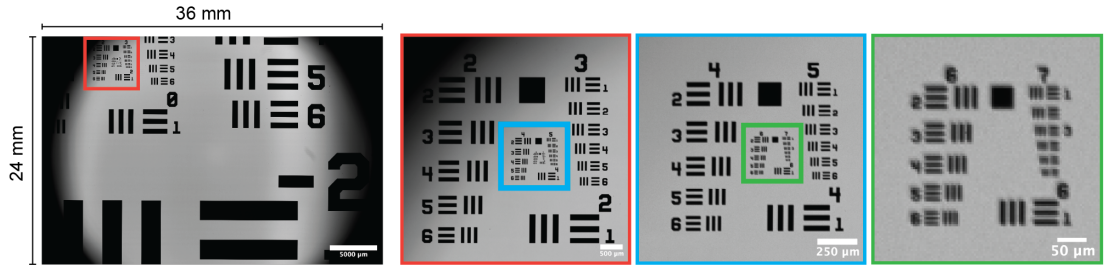

Fig. S2. Bright-field image of USAF-1951 test target centered and brought to focus near the edge of the macroscope's filed of view.

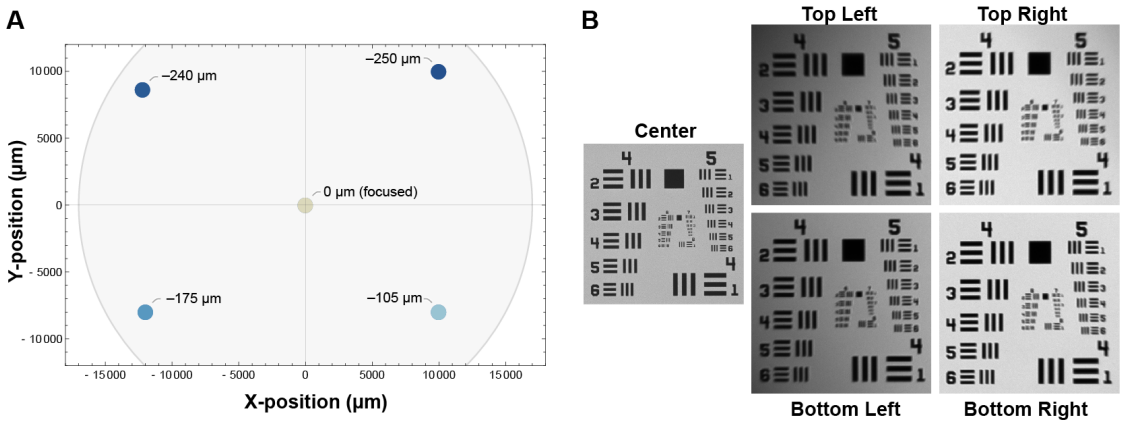

Fig. S3. Characterizing field curvature of the macroscope. (A) Apparent axial displacement of the field at different positions (colored points) near the periphery of the usable FOV (approximated by the gray circular region) relative to best-focus at a position at approximately the center (beige point), as determined with a USAF-1951 resolution test target. (B) Images of a USAF-1951 test target at positions relative to the usable FOV, showing loss of resolution near the periphery when at an axial position corresponding to best focus at the center of the FOV.

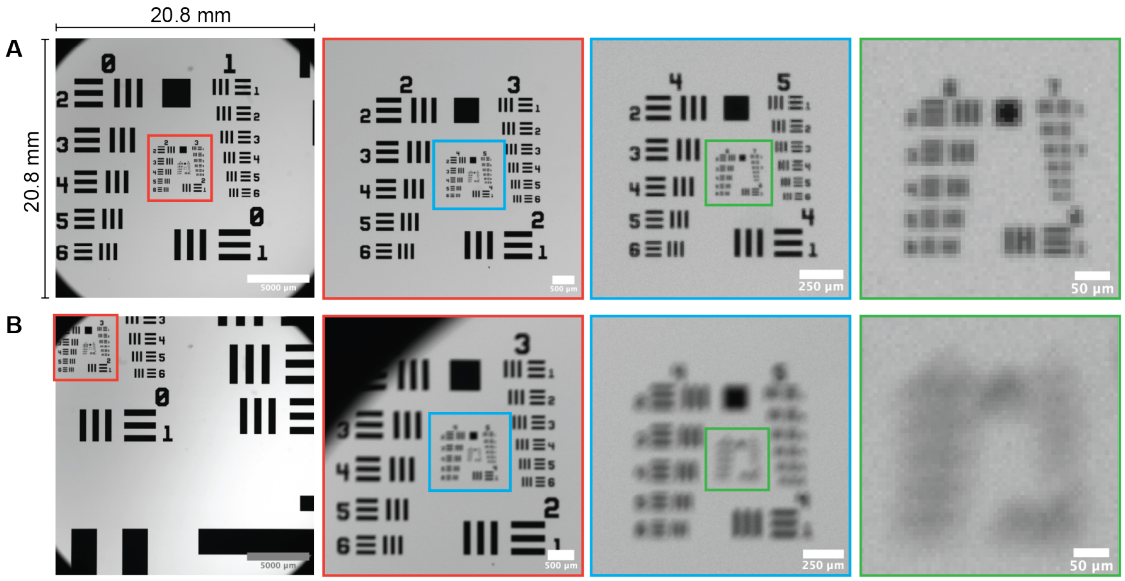

Fig. S4. Bright-field image of USAF-1951 test target on a Nikon Ti2 microscope equipped with a 1X objective, with target positioned at the center (A) or edge (B) of the field of view and focused (to best focus) at the center and edge of the FOV, respectively.

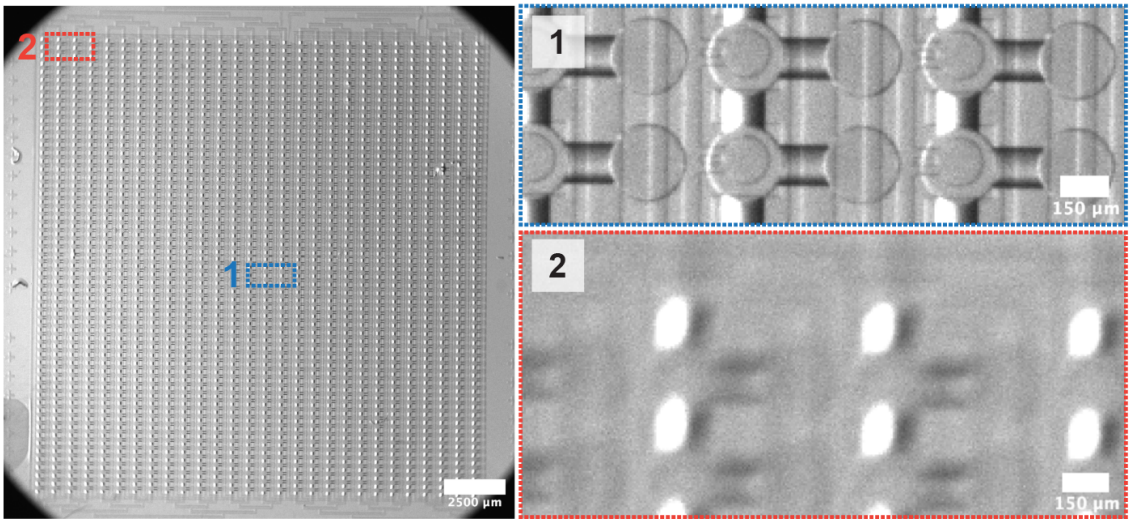

Fig. S5. Bright-field image of the HT-MEK device acquired with the Ti2 equipped with 1X objective, focused at the center of the FOV.

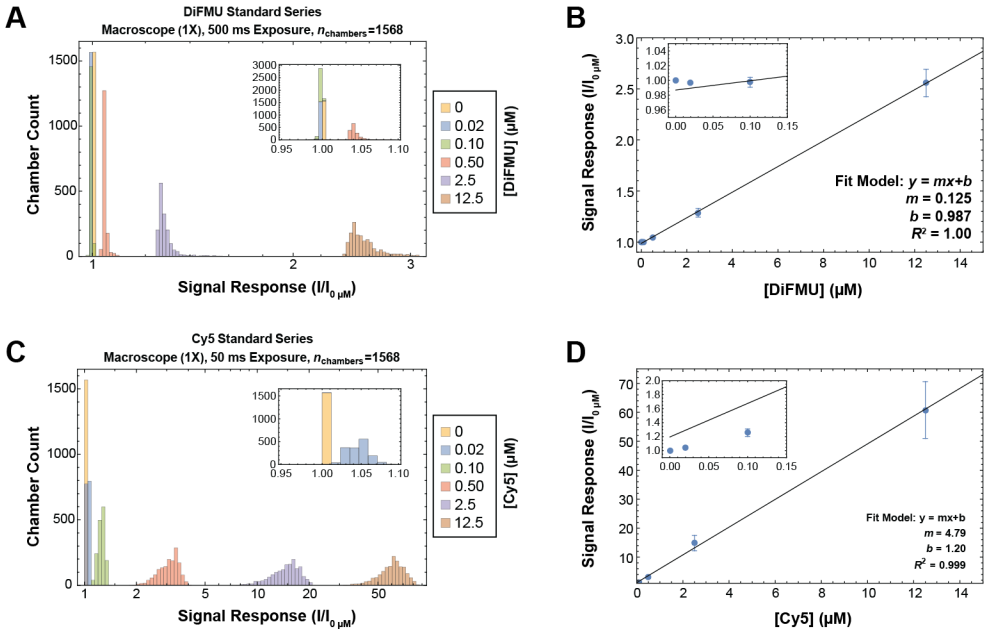

Fig. S6. DAPI and Cy5 standard curves on an HT-MEK device acquired with the macroscope. (A & C) Binned histogram of median chamber intensities of DiFMU and Cy5 standard series, respectively, normalized to background intensity on a per-chamber basis. (B & D) Linear fit to mean of signal response from panels (A) & (C), respectively, across all chambers. All error bars are ±1 SD from the mean.

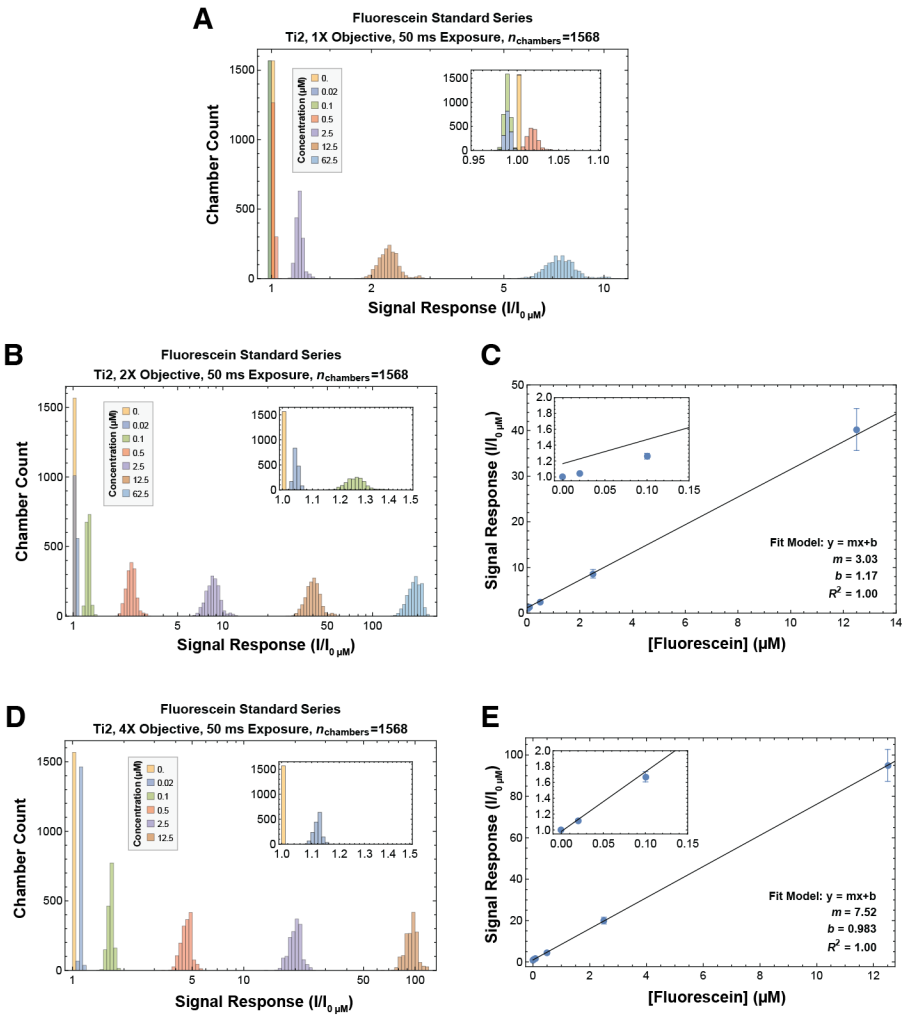

Fig. S7. Fluorescein standard curves on an HT-MEK device acquired with a Ti2-based imaging system. (A, B, & D) Binned histogram of median chamber intensities of fluorescein standard series obtained with a 1X, 2X, and 4X objective, respectively, normalized to background intensity on a per-chamber basis. (C & E) Linear fit to mean of signal response from panels (B) & (D), respectively, across all chambers. All error bars are ±1 SD from the mean.

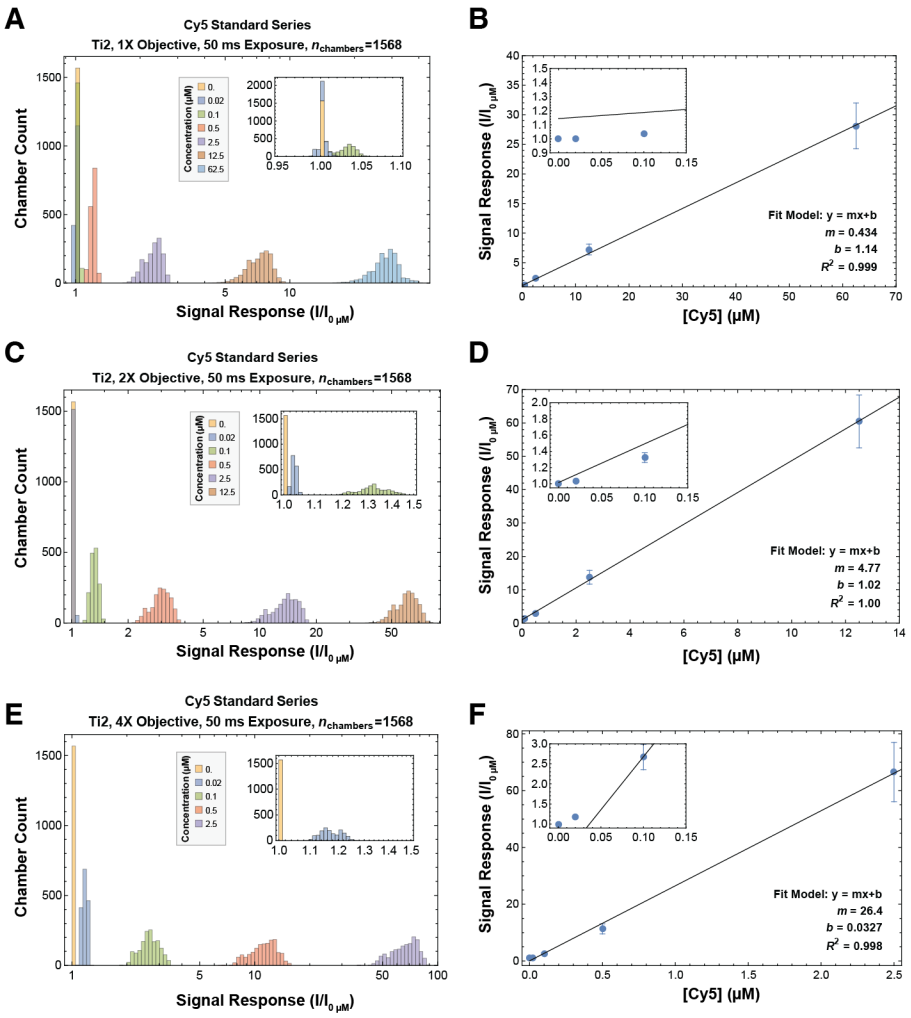

Fig. S8. Cy5 standard curves on an HT-MEK device acquired with a Ti2-based imaging system. (A, C, & E) Binned histogram of median chamber intensities of Cy5 standard series obtained with a 1X, 2X, and 4X objective, respectively, normalized to background intensity on a per-chamber basis. (B, D, & F) Linear fit to mean of signal response from panels (A), (C) & (E), respectively, across all chambers. All error bars are ±1 SD from the mean.

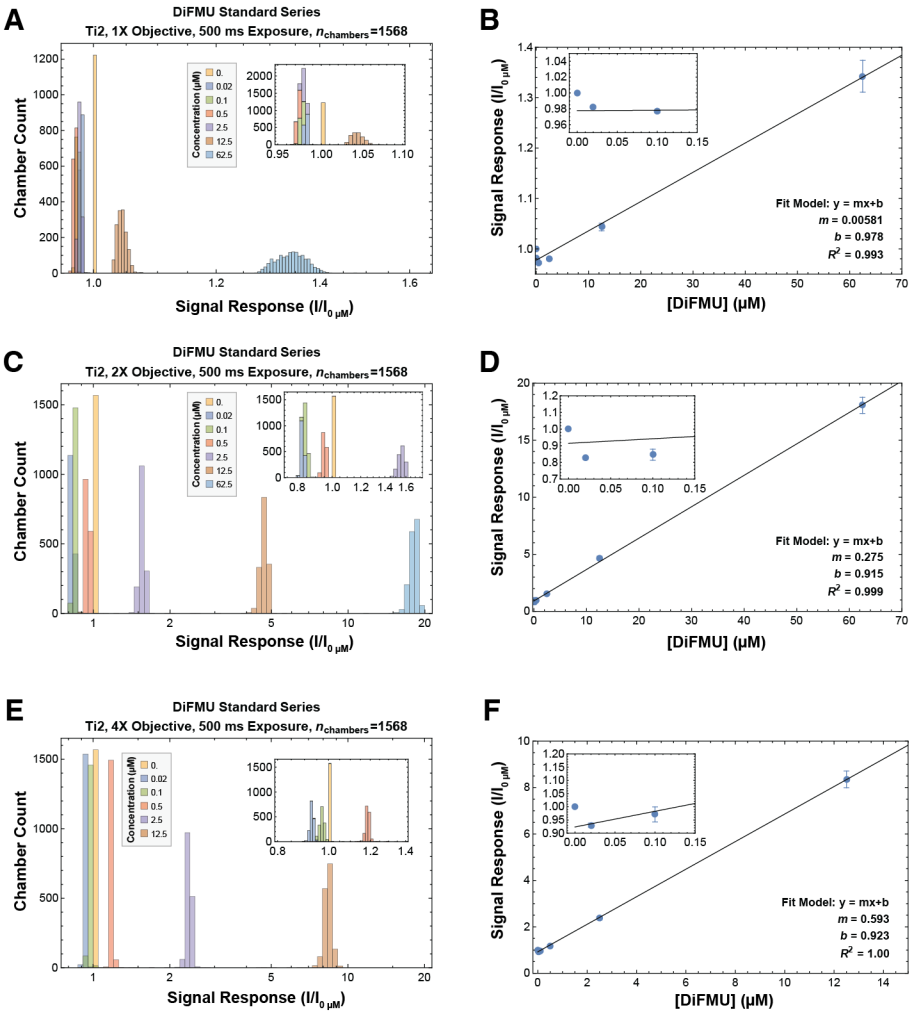

Fig. S9. DiFMU standard curves on an HT-MEK device acquired with a Ti2-based imaging system. (A, C, & E) Binned histogram of median chamber intensities of DiFMU standard series obtained with a 1X, 2X, and 4X objective, respectively, normalized to background intensity on a per-chamber basis. (B, D, & F) Linear fit to mean of signal response from panels (A), (C) & (E), respectively, across all chambers. All error bars are ±1 SD from the mean.

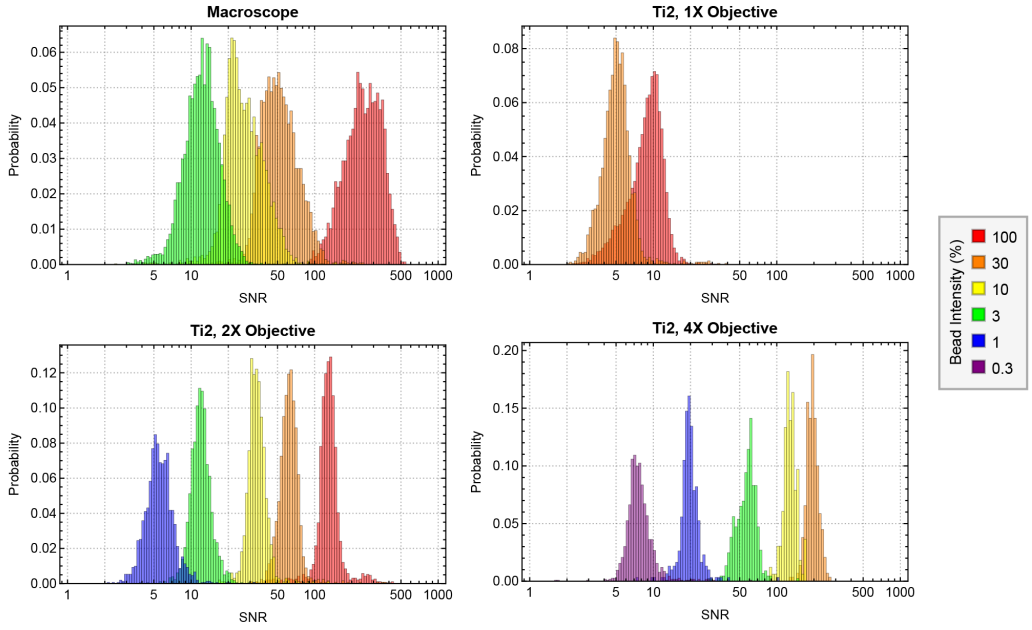

Fig. S10. Distributions of signal-to-noise ratio (SNR) for fluorescent calibration bead particles (Thermo Fisher InSpeck Green, 6 µm particles, cat. no. I14785) over their local backgrounds on the macroscope and Ti2 comparison system. All images were acquired with 40 ms exposure in the GFP channel. Hundreds to thousands of particles were quantified per distribution, and bins were normalized to give probability distributions. Beads at low intensities omitted from analyses could not be reliably thresholded above background, and 100% intensity beads were omitted from analysis of images from the Ti2 with 4X objective analysis because they saturated the sensor.

Tables S1 to S5

Component	Subcomponent	Manufacturer	Vendor	Part Name	Manufacturer SKU	Count	Unit Price (as built)	Total Price (as built)	Total Price (all new)	Note
Camera	–	ZWO	Agena Astro	ASI6200MM	ASI6200MM-P	1	$3,799.00	**$3,799.00**	**$3,799.00**	
Lens system	Lens	Rokinon	Amazon	Rokinon Series II 85mm F1.4 Lens	SE85AE-N	2	$279.00	$558.00		
Lens system	Coupler	PreciseParts	PreciseParts	Custom ZWO EFW 5x2 filter wheel M54 to generic filter 72 mm	–	2	$116.00	$232.00		
							Component Total	**$790.00**	**$790.00**	
Stage	Motion Control	ASI	Ebay	MS-2000 Small XY Stage (Second Hand)	MS-2000	1	$1,000.00	$1,000.00	$7,150.00	New Part: MS-2000 Small XY Stage
Stage	Motion Control	ASI	Ebay	LS-50 Linear Stage (Second Hand)	LS-50	1	$750.00	$750.00	$2,250.00	New Part: LS-50 Linear Stage
Stage	Motion Control	ASI	ASI	LX-4000 Controller (Second Hand)	LX-4000	1	$750.00	$750.00	$4,725.00	New Part: MS-2000 Controller (MS3)
Stage	Motion Control	Xometry	Xometry	Laser cut stage bracket, aluminum	–	1	$57.69	$57.69		
Stage	Stage Insert	Xometry	Xometry	Laser cut stage insert, aluminum	–	1	$29.32	$29.32		
Stage	Stage Insert	Xometry	Xometry	Laser cut stage retainers, aluminum	–	2	$13.51	$27.02		
Stage	Stage Insert	–	–	3D-printed slide clamp, ABS plastic	–	6	–	–		Printed in house at nominal cost
Stage	Stage Insert	McMaster-Carr	McMaster-Carr	18-8 Stainless Steel Socket Head Screw, 2-56 Thread Size, 5/16" Long	92196A078	14	$0.08	$1.12		
Stage	Stage Insert	McMaster-Carr	McMaster-Carr	18-8 Stainless Steel Socket Head Screw, 2-56 Thread Size, 5/32" Long	92196A075	6	$0.09	$0.54		
Stage	Stage Insert	McMaster-Carr	McMaster-Carr	18-8 Stainless Steel Coupling Nut, 2-56 Thread Size	90268A203	6	$2.42	$14.52		
Stage	Stage Insert	McMaster-Carr	McMaster-Carr	18-8 Stainless Steel Nylon-Tip Set Screw, 2-56 Thread Size, 3/16" Long	90291A847	4	$1.26	$5.04		
Stage	Stage Insert	McMaster-Carr	McMaster-Carr	18-8 Stainless Steel Narrow Hex Nut, 2-56 Thread Size	90730A003	8	$0.04	$0.32		
							Component Total	**$2,635.57**	**$14,260.57**	
Light path	Filter wheel	ZWO	Agena Astro	ZWO EFW (5 x 2")	EFW-5x2	2	$299.00	$598.00		
Light path	Filter wheel	–	–	3D-printed filter cell, ABS plastic	–	5	–	–		Printed in house at nominal cost
Light path	Filter wheel	–	–	3D-printed filter cell spacer, ABS plastic	–	5	–	–		
Light path	Excitation Filter	Chroma Technology	Chroma Technology	ET376/30x 50mm Dia Mounted 2.3mm thick ring	ET376/30x	1	$865.00	$865.00		
Light path	Excitation Filter	Chroma Technology	Chroma Technology	ET470/40x 50mm Dia Mounted 2.3mm thick ring	IN100494	1	$825.00	$825.00		
Light path	Excitation Filter	Chroma Technology	Chroma Technology	ET620/60x 50mm Dia Mounted 2.3mm thick ring	ET620/60x	1	$865.00	$865.00		
Light path	Excitation Filter	Thorlabs	Thorlabs	Unmounted Ø2" Absorptive ND Filter, OD 2.0	NE2R20B	1	$93.18	$93.18		
Light path	Emission Filter	Chroma Technology	Chroma Technology	ET450/50m 50mm Dia Mounted 2.3mm thick ring	ET450/50m	2	$865.00	$1,730.00		
Light path	Emission Filter	Chroma Technology	Chroma Technology	ET525/36m 50mm Dia Mounted 2.3mm thick ring	IN044448	2	$825.00	$1,650.00		
Light path	Emission Filter	Chroma Technology	Chroma Technology	ET690/50m 50mm Dia Mounted 2.3mm thick ring	ET690/50m	2	$865.00	$1,730.00		
							Component Total	**$8,356.18**	**$8,356.18**	
Light path	Collimator	Thorlabs	Thorlabs	Ø3 mm LLG to SM1 Adapter	AD3LLG	1	$38.32	$38.32		
Light path	Collimator	Thorlabs	Thorlabs	SM1 Lens Tube Sleeve 1.5" Long	SM1M15	1	$19.84	$19.84		
Light path	Collimator	Thorlabs	Thorlabs	Thick SM05 Int. to SM1 Ext. Adapter	SM1A6T	1	$23.41	$23.41		
Light path	Collimator	Thorlabs	Thorlabs	1/2" retaining ring	SM05RR	1	$4.33	$4.33		
Light path	Collimator	Thorlabs	Thorlabs	Ø12.7mm, F=8mm, Aspherical Condenser lens, AR coated	ACL12708U-A	1	$31.77	$31.77		
Light path	Collimator	Thorlabs	Thorlabs	Fly's Eye Homogenizer, Uncoated, WD=95mm	FLE2	1	$813.96	$813.96		
							Component Total	**$931.63**	**$931.63**	
Body	Base	Thorlabs	Thorlabs	Aluminum Breadboard 24" x 36" x 1/2", 1/4"-20 Taps	MB2436	1	$793.11	$793.11		
Body	Support	Thorlabs	Thorlabs	95 mm Construction Rail, Clear Anodized, L = 750 mm	XT95-750	1	$220.11	$220.11		
Body	Support	Thorlabs	Thorlabs	Base Plate for 95 mm Rails	XT95P3	2	$58.82	$117.64		
Body	Support	Thorlabs	Thorlabs	95 mm Rail Construction Clamp, 1/4"-20 Locking Screw	XT95P13	1	$122.28	$122.28		
Body	Support	Thorlabs	Thorlabs	Fixed Arm, Internal SM2 Threads, 60 mm Cage Compatible	CSA1002	2	$351.72	$703.44		
Body	Bracket	Thorlabs	Thorlabs	Right-Angle Bracket for 50 mm Rails	XE50A90	1	$74.27	$74.27		
Body	Tube	Thorlabs	Thorlabs	SM2 Lens Tube, 0.5" Thread Depth	SM2L05	1	$28.42	$28.42		
Body	Light Stop	Thorlabs	Thorlabs	SM3 Ring-Actuated Iris Diaphragm (Ø2.5 - Ø50.0 mm)	SM3D50D	1	$156.99	$156.99		
Body	Adapters	Thorlabs	Thorlabs	Adapter with External SM2 Threads and Internal SM3 Threads	SM3A2	1	$35.35	$35.35		
Body	Adapters	Thorlabs	Thorlabs	Male SM2 to Female F-mount Ring	SM2NFMA	1	$108.41	$108.41		
Body	Adapters	Thorlabs	Thorlabs	Male M54x0.75 to Female SM2	SM2A28	3	$34.17	$102.51		
Body	Adapters	Thorlabs	Thorlabs	Male SM2 to Male SM2	SM2T2	2	$41.29	$41.29		
Body	Fasteners	Thorlabs	Thorlabs	1/4"-20 Cap Screw and Hardware Kit	HW-KIT2	1	$139.58	$139.58		Only a subset required for build
							Component Total	**$2,643.40**	**$2,643.40**	
							Subtotal	**$19,155.78**	**$30,780.78**	
Light Source	Illumination	Lumencor	Lumencor	SPECTRA III Light Engine	90-10508	1	$22,585.50	**$22,585.50**	**$22,585.50**	
							Grand Total	**$41,741.28**	**$53,366.28**	

Table S1. Build list of the transfluorescence macroscope imaging system described herein.

Setup	Lens Type	Magnification	Component	Model No.	Vendor	Manufacturer	Image Circle Ø (mm)	Numerical Aperture	Working distance (mm)	Notes
Macroscope	Tandem-Lens Macro	1X	Custom Coupled Rokinon 85mm f/1.4 Series II Lenses	–	–	–	34	~0.2–0.3	34	a, b
Ti2	Objective	1X	CFI Plan Achro 1X	MRL00012	Nikon	Nikon	26	0.04	3.2	c, d
Ti2	Objective	2X	CFI Plan Apochromat Lambda D 2X	MRD70020	Nikon	Nikon	> 14.7	0.1	8.5	c, d
Ti2	Objective	4X	CFI Plan Apochromat Lambda D 4X	MRD70040	Nikon	Nikon	> 7.3	0.2	20	c, e

Notes

a Working distance when used in the configuration specified in this build

b The nominal numerical aperature of the macroscope is estimated as follows: NA ≈ n*(D/2f) = 1*(50 mm)/(2*85mm) = 0.29
where n = index of refraction, D = effective entrance pupil diameter (in our system, the clipping from the 50 mm filter wheel aperature is likely limiting actual NA), and f = lens focal length.
Other lens factors including internal aperatures or large pupil magnification may limit actual NA further, so we estimate, leading to an estimate between approximately 0.2–0.3

c Working distance define as distance front metal housing to focal plane

d Apparent image circle diameter defined by border of hard-vignetting

e Image circle covers the full sensor, so the image circle is a lower limit

Table S2. Comparison of macroscope tandem lens system and object lenses of the Nikon Ti2 comparison system. All Nikon objectives compared were of the highest NA commercially available.

Setup	Channel	Component	Assembly Name	Vendor	Manufacturer	SKU	Spectral properties	Spectral properties description	Mount
Macroscope	DAPI	Excitation Bandpass Filter	–	Chroma Technology	Chroma Technology	ET376/30x (IN103920)	376/30	Center Wavelength (nm) / FWHM Bandwidth (nm)	Custom filter cell
Macroscope	DAPI	Emission Bandpass Filter	–	Chroma Technology	Chroma Technology	ET450/50m (IN103922)	450/50	Center Wavelength (nm) / FWHM Bandwidth (nm)	Custom filter cell
Macroscope	GFP	Excitation Bandpass Filter	–	Chroma Technology	Chroma Technology	ET470/40x (IN100494)	470/40	Center Wavelength (nm) / FWHM Bandwidth (nm)	Custom filter cell
Macroscope	GFP	Emission Bandpass Filter	–	Chroma Technology	Chroma Technology	ET525/36m (IN044448)	525/36	Center Wavelength (nm) / FWHM Bandwidth (nm)	Custom filter cell
Macroscope	CY5	Excitation Bandpass Filter	–	Chroma Technology	Chroma Technology	ET620/60x (IN101685)	620/60	Center Wavelength (nm) / FWHM Bandwidth (nm)	Custom filter cell
Macroscope	CY5	Emission Bandpass Filter	–	Chroma Technology	Chroma Technology	ET690/50m (IN101686)	690/50	Center Wavelength (nm) / FWHM Bandwidth (nm)	Custom filter cell
Ti2	DAPI	Excitation Bandpass Filter	DAPI SOLA Filter Cube	Nikon	Semrock	FF01-378/52	378/52	Center Wavelength (nm) / FWHM Bandwidth (nm)	Filter cube
Ti2	DAPI	Dichroic Beamsplitter	DAPI SOLA Filter Cube	Nikon	Semrock	FF409-Di03	409	Cut-on wavelength (nm)	Filter cube
Ti2	DAPI	Emission Bandpass Filter	DAPI SOLA Filter Cube	Nikon	Semrock	FF02-447/60	447/60	Center Wavelength (nm) / FWHM Bandwidth (nm)	Filter cube
Ti2	GFP	Excitation Bandpass Filter	GFP Filter Cube	Nikon	Semrock	FF01-466/40	466/40	Center Wavelength (nm) / FWHM Bandwidth (nm)	Filter cube
Ti2	GFP	Dichroic Beamsplitter	GFP Filter Cube	Nikon	Semrock	FF495-Di03	495	Cut-on wavelength (nm)	Filter cube
Ti2	GFP	Emission Bandpass Filter	GFP Filter Cube	Nikon	Semrock	DD03-525/50	525/50	Center Wavelength (nm) / FWHM Bandwidth (nm)	Filter cube
Ti2	CY5	Excitation Bandpass Filter	Cy5 Filter Cube	Nikon	Semrock	FF01-618/50	618/50	Center Wavelength (nm) / FWHM Bandwidth (nm)	Filter cube
Ti2	CY5	Dichroic Beamsplitter	Cy5 Filter Cube	Nikon	Semrock	FF652-Di01	652	Cut-on wavelength (nm)	Filter cube
Ti2	CY5	Emission Bandpass Filter	Cy5 Filter Cube	Nikon	Semrock	FF01-698/70	698/70	Center Wavelength (nm) / FWHM Bandwidth (nm)	Filter cube

Table S3. Filters and dichroic mirrors used in the macroscope and Ti2 comparison system.

			Bead Fluorescence Intensity (%), Mean SNR					
Setup	**Channel**	**Exposure (ms)**	**100**	**30**	**10**	**3**	**1**	**0.3**
Macroscope	GFP	40	250	55	28	12	—	—
Ti2, 1X	GFP	40	8.5	5.1	—	—	—	—
Ti2, 2X	GFP	40	130	63	34	12	5.6	—
Ti2, 4X	GFP	40	—	200	130	57	20	7.9

Table S4. Mean SNRs of fluorescent beads (Thermo Fisher, InSpeck Green) imaged on the macroscope and Ti2 comparison system. Missing values correspond to bead intensity that saturated the imaging sensor at the exposure time chosen (100% intensity on the Ti2 with 4X objective) or at which beads could not be reliably thresholded over background (all other missing values).

Setup	Objective	Channel	LightSource	Recorded Power (mW)	Beam Coverage	Beam Dimensions	Beam Area (mm2)	Sensor Illuminated Area (mm2)	Sensor Area (mm2)	Beam Profile Estimate	Estimated Density (mW/cm2)	Estimated Total Output (mW)
Macroscope	–	dapi	SPECTRA III	61	Full sensor	29 mm x 35 mm	1015	324	324	Flat Top	19	193
Macroscope	–	gfp	SPECTRA III	60	Full sensor	29 mm x 35 mm	1015	324	324	Flat Top	19	193
Macroscope	–	cy5	SPECTRA III	42	Full sensor	29 mm x 35 mm	1015	324	324	Flat Top	13	132
Ti2	1X	dapi	SOLA	27	Full sensor	∅26mm	531	324	324	Flat Top	8	42
Ti2	1X	gfp	SOLA	141	Full sensor	∅26mm	531	324	324	Flat Top	44	234
Ti2	1X	cy5	SOLA	104	Full sensor	∅26mm	531	324	324	Flat Top	32	170
Ti2	2X	dapi	SOLA	30	Circular subset of sensor	∅14mm	154	154	324	Flat Top	19	29
Ti2	2X	gfp	SOLA	270	Circular subset of sensor	∅14mm	154	154	324	Flat Top	175	270
Ti2	2X	cy5	SOLA	218	Circular subset of sensor	∅14mm	154	154	324	Flat Top	142	219
Ti2	4X	dapi	SOLA	36	Circular subset of sensor	∅8mm	50	50	324	Flat Top	72	36
Ti2	4X	gfp	SOLA	308	Circular subset of sensor	∅8mm	50	50	324	Flat Top	616	308
Ti2	4X	cy5	SOLA	246	Circular subset of sensor	∅8mm	50	50	324	Flat Top	492	246
Ti2	1X	dapi	SPECTRA III	23	Full sensor	∅26mm	531	324	324	Flat Top	7	37
Ti2	1X	gfp	SPECTRA III	105	Full sensor	∅26mm	531	324	324	Flat Top	32	170
Ti2	1X	cy5	SPECTRA III	129	Full sensor	∅26mm	531	324	324	Flat Top	40	212
Ti2	2X	dapi	SPECTRA III	24	Circular subset of sensor	∅14mm	154	154	324	Flat Top	16	25
Ti2	2X	gfp	SPECTRA III	196	Circular subset of sensor	∅14mm	154	154	324	Flat Top	127	196
Ti2	2X	cy5	SPECTRA III	254	Circular subset of sensor	∅14mm	154	154	324	Flat Top	165	254
Ti2	4X	dapi	SPECTRA III	29	Circular subset of sensor	∅8mm	50	50	324	Flat Top	58	29
Ti2	4X	gfp	SPECTRA III	221	Circular subset of sensor	∅8mm	50	50	324	Flat Top	442	221
Ti2	4X	cy5	SPECTRA III	276	Circular subset of sensor	∅8mm	50	50	324	Flat Top	552	276

Table S5. Measured excitation light power of the macroscope and Ti2 systems for each channel and objective lens used in this study. Measurements were made using a Thorlabs S175C thermal power sensor and Thorlabs PM100A power meter. For measurements on the macroscope, the focus target (back) of the sensor was brought to focus, then the target was moved down by 4.8 mm (the sensor thickness) to bring the active sensor surface to the focal plane. For measurements on the Ti2, the system was focused on the back of the sensor, then the sensor was flipped over to measure power at the focal plane.

References

1. Applied scientific instrumentation. https://asiimaging.com/docs/ls50 (accessed Spring 2024).

2. E. H. Ratzlaff, A. Grinvald, *J. Neurosci. Methods* **36**, 127 (1991).

3. A. D. Edelstein, *et al.*, *J. Biol. Methods* **1**, e10 (2014).

4. C. J. Markin, *et al.*, *Science* **373**, eabf8761 (2021).

5. C. A. Werley, M.-P. Chien, A. E. Cohen, *Biomed. Opt. Express.* **8**, 5794 (2017).

6. P. M. Fordyce, *et al.*, *Nat. Biotechnol.* **28**, 970 (2010).

7. K. Brower, *et al.*, *HardwareX* **3**, 117 (2018).

8. M. Model, *Curr. Protoc. Cytom.* **68**, 10.14.1 (2014).